The International Journal of Advanced Manufacturing Technology (2022) 121:6431–6438
https://doi.org/10.1007/s00170-022-09741-9

ORIGINAL ARTICLE

Ductile regime grinding of silicon nitride ceramics based on dynamic critical grinding depth

Wei Liu[1] · Dubo Tang[1] · Rentong Liu[1] · Zhaohui Deng[1] · Hao Gu[1] · Shun Liu[1]

Received: 25 January 2022 / Accepted: 7 July 2022 / Published online: 20 July 2022

Abstract

Considering both the grinding parameters and dynamic mechanical properties of the silicon nitride ceramics, the dynamic critical grinding depth model of the ductile regime grinding was established. The grinding experiment of the silicon nitride ceramics was carried out on a surface grinder MGK7120×6/F. The grinding force was compared with the critical load for the cracking, then the material removal mode was analyzed. The pixel mesh method was used to calculate the proportion of the brittle regime, and the material removal mode was further validated. The material removal mode of the silicon nitride ceramic grinding was predicted using the maximum undeformed grinding thickness model and dynamic critical grinding depth model. The predicted results were consistent with the results of the experimental analysis, and the correctness of the dynamic critical grinding depth model of the ductile regime grinding was verified. The mechanism of the grinding strain rate on the material removal mode was analyzed, and it was found that increasing the strain rate was conducive to achieving the ductile material removal, then improving the grinding quality. The research is useful to optimize the grinding parameters to reduce the damage in the ceramic grinding.

Keywords Silicon nitride ceramic · Strain rate · Ductile regime · Dynamic critical grinding depth

1 Introduction

Silicon nitride (Si_3N_4) ceramics have been widely used in machinery, chemicals, electronics, energy, metallurgy, national defense, and aerospace due to their excellent thermal and mechanical properties. At present, grinding is the main processing method for the engineering ceramics. The ceramic grinding can easily cause the surface and subsurface damage because of its inherent hardness and brittleness. Besides, the quality of the machined surface is difficult to guarantee [1]. To achieve the high accuracy and reduce the grinding damage, the ductile regime grinding is the preferred method [2].

Many scholars have studied the mechanism of brittle-to-ductile transition of the brittle materials' grinding [3, 4]. With the single-point diamond cutting of the silicon and germanium, Blake and Scattergood [5] found that the critical chip depth was the best parameter to evaluate the influence of the grinding parameters on the ductile regime machining. According to the Griffith fracture criterion and indentation test, a classical critical depth model of the brittle-ductile transition for brittle materials was proposed [3]. The brittle materials can be removed in the ductile regime only when the grinding depth is less than the critical depth. Venkatachalam et al. [6] established the critical undeformed chip thickness model and realized the ductile regime grinding of single-crystal silicon. Chen et al. [7] studied the critical conditions for the brittle-to-ductile transition of brittle materials in dynamic grinding. Considering the size effect factor and micro-grinding tool topography, Cheng et al. [8] presented a mathematical model of the undeformed chip thickness to describe the ductile regime in the micro-grinding. Ma et al. [9] developed the critical grinding depth models of the ductile-ductile brittle and ductile brittle-brittle for the machinable glass ceramics. Pratap et al. [10] investigated the material removal mechanism of the BK7 glass and determined the critical chip thickness to fabricate the parallel and intersecting micro-slots. All the above researches indicate that

✉ Wei Liu
lw1986tiger@163.com

[1] Hunan Provincial Key Laboratory of High Efficiency and Precision Machining of Difficult-to-Cut Material, School of Mechanical Engineering, Hunan University of Science and Technology, Hunan Province, Xiangtan 411201, China

the ductile regime removal can be achieved in the brittle materials' grinding as in the machining of the metallic materials.

For the grinding of Si_3N_4, the material removal in the machining zone is mostly a mixed-mode of ductile and brittle [11, 12]. The quality of the machined surface can be improved by increasing the proportion of the ductile regime removal [13]. Therefore, it is essential to study the critical grinding depth of the brittle-ductile transition of Si_3N_4. Based on the classical critical grinding depth model, a dynamic critical grinding depth model was established considering both the grinding parameters and dynamic material mechanical properties, while the grinding parameters include the grinding wheel speed, grinding depth, and workpiece speed. Furthermore, the correctness of the model was verified by the analysis of the Si_3N_4 grinding experiments with different grinding parameters.

2 The establishment of a dynamic critical grinding depth model

2.1 Maximum undeformed grinding thickness model

The maximum undeformed grinding thickness a_{gmax} of a single abrasive grain in the surface grinding is shown in Fig. 1 [14]. The diameter of the grinding wheel is d_s, the grinding wheel speed is v_s, the grinding depth is a_g, and the workpiece speed is v_w. It can be seen from Fig. 1 that the undeformed grinding thickness is constantly changed from small to large and then to small. A mathematical model of a_{gmax} is developed, as shown in Eq. (1) [15].

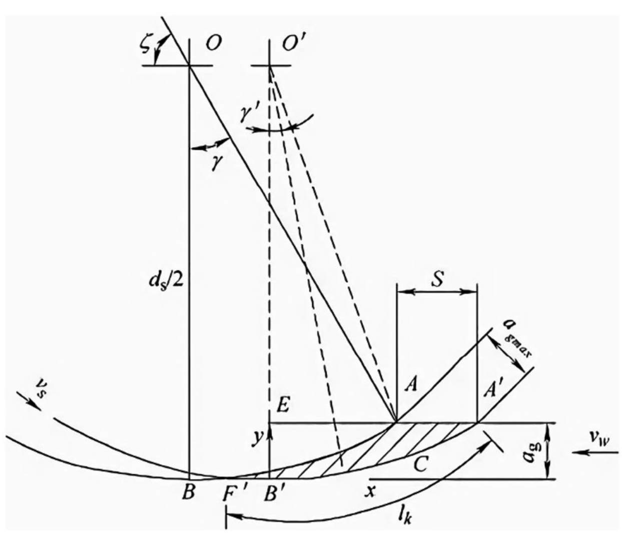

Fig. 1 Maximum undeformed grinding thickness for single grain grinding

$$a_{\mathrm{gmax}} = 2\lambda\left(\frac{v_w}{v_s}\right)\left(\frac{a_g}{d_s}\right)^{\frac{1}{2}} \tag{1}$$

where λ is the inter-grain spacing, which is related to the grinding depth and grinding wheel parameters.

2.2 Dynamic critical grinding depth model

Based on the Griffith fracture propagation criterion and the effective measure of brittleness in indentation, the classical critical grinding depth a_c is [3]:

$$a_c = \Psi(\frac{K_{IC}}{H})^2(\frac{E}{H}) \tag{2}$$

where E is the Young's modulus, H is the hardness, K_{IC} is the static fracture toughness, and Ψ is a dimensionless constant which is equal to 0.15 for ceramic materials [16].

The classical critical grinding depth model only considers the static mechanical properties of materials. But the grinding process is a high-speed dynamic machining process, so the mechanical properties of materials will be significantly changed for the strain rate effect [17, 18]. Therefore, the actual critical grinding depth in the ductile regime is significantly different from the traditional theory [5]. The mathematical relationship between the critical grinding depth a_{gd} and the dynamic fracture toughness K_{ID} and hardness H is as shown in Eq. (3) [15].

$$a_{gd} = \frac{2\ \sin^4\ \theta}{\pi}\cot\ \theta(\frac{K_{ID}}{H})^2(\frac{E}{H})^{\frac{1}{2}} \tag{3}$$

where θ is the half-angle of the diamond indenter cone apex, and the value is mostly 60° [15].

In the grinding process, the change of the grinding parameters will affect the strain rate of the grinding zone and ultimately affect the fracture toughness of the material. The relationship between K_{ID} and K_{IC} is as follows [2]:

$$K_{ID} = (a + b\ \ln\ \dot{\varepsilon})K_{IC} \tag{4}$$

where a and b are the material constants and $\dot{\varepsilon}$ is the strain rate, which can be obtained by the Hopkinson experiment [19]. The values of a and b are − 14.95 and 0.86 for Si_3N_4 ceramic material, respectively. The relationship between a_{gd} and $\dot{\varepsilon}$ can be expressed as Eq. (5).

$$a_{gd} = \frac{2\ \sin^4\ \theta}{\pi}\cot\ \theta\left[\frac{\left(a + b\ \ln\ \dot{\varepsilon}\right)K_{IC}}{H}\right]^2\left(\frac{E}{H}\right)^{\frac{1}{2}} \tag{5}$$

From Eq. (5), it can be seen that a_{gd} is not a fixed value, but increases with the increasing of $\dot{\varepsilon}$. $\dot{\varepsilon}$ can be expressed as [20]

Table 1 Mechanical properties of silicon nitride ceramics

Density (g/cm^3)	Elastic modulus (GPa)	Microhardness (GPa)	Fracture toughness ($MPa \cdot m^{1/2}$)	Yield strength (MPa)
3.2	320	17.4	6.8	700

$$\dot{\varepsilon} = \frac{v_s}{l_s} \tag{6}$$

where l_s is the contact length between the abrasive grain and workpiece. It can be expressed as $l_s = Ka_{gmax}$. K is a constant related to the shape of the grinding wheel and workpiece material. The value of K is 0.6–0.9 [21].

Therefore, by substituting Eq. (6) into Eq. (5), a dynamic critical grinding depth model considering the grinding parameters and material mechanical properties can be obtained. Where $c = a - bln(K)$.

$$a_{gd} = \frac{2\ \sin^4\ \theta}{\pi} \cot\ \theta \cdot [c + b \ln (\frac{v_s^2}{2\lambda v_w} \sqrt{\frac{d_s}{a_g}})]^2 (\frac{K_{IC}}{H})^2 (\frac{E}{H})^{\frac{1}{2}} \tag{7}$$

It can be seen from Eq. (7) that v_s has the most obvious influence on a_{gd}, followed by v_w and a_g.

3 Grinding experiment

3.1 Experimental material

The workpiece material used in the grinding experiment is the Si_3N_4 ceramic material. The workpiece is a square block with the size of 20 mm × 20 mm × 10 mm, which is made by the air pressure sintering. Figure 2 shows the Si_3N_4 workpiece and its microstructure. Figure 2a shows the workpiece, while (b) and (c) show the microstructure observed by a digital microscope and SEM, respectively. The crystal form of the material is mostly granular, with uniform and dense microstructure and small grain size. The main mechanical properties of Si_3N_4 are shown in Table 1.

3.2 Experimental equipment

The Si_3N_4 grinding experiment was performed on a CNC high precision surface grinding machine MGK7120 × 6/F, using a resin-bonded diamond grinding wheel with a size of 200 mm × 32 mm × 15 mm. Figure 3 shows the grinding experimental system. The grinding force was measured using a piezoelectric dynamometer Kistler 9257B. The surface morphology of the workpiece was observed by a digital microscope VHX-500FE and a scanning electron microscope FEI Quanta 200. The surface roughness of the

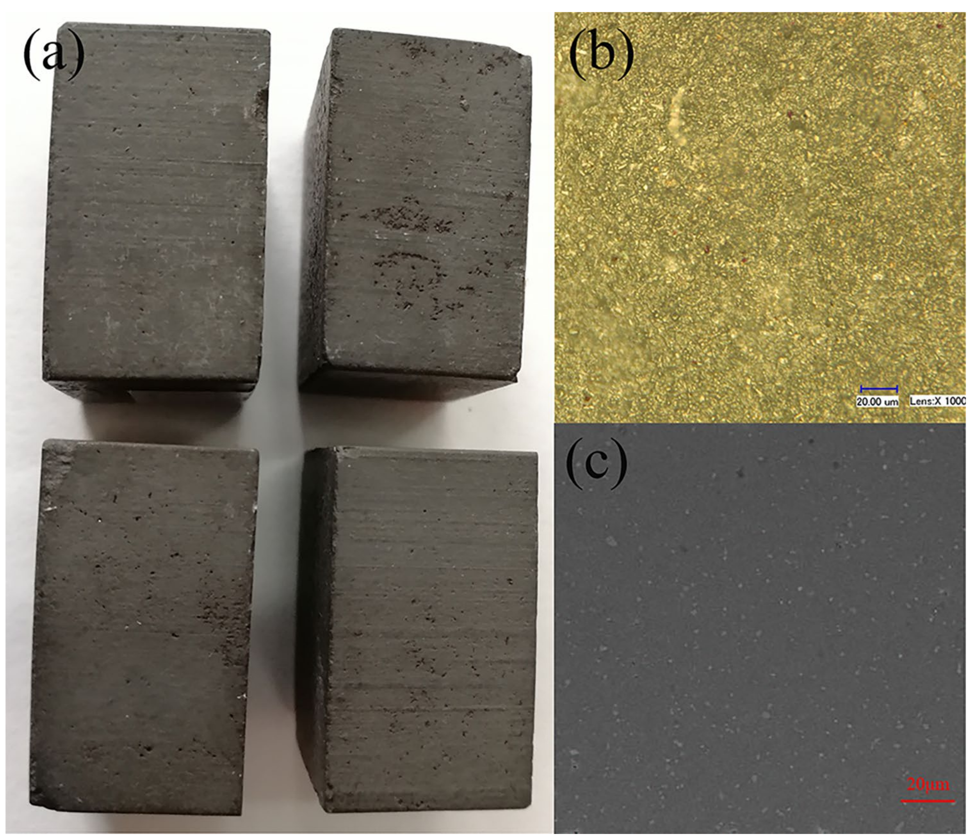

Fig. 2 **a** Silicon nitride workpieces and **b**, **c** microstructure

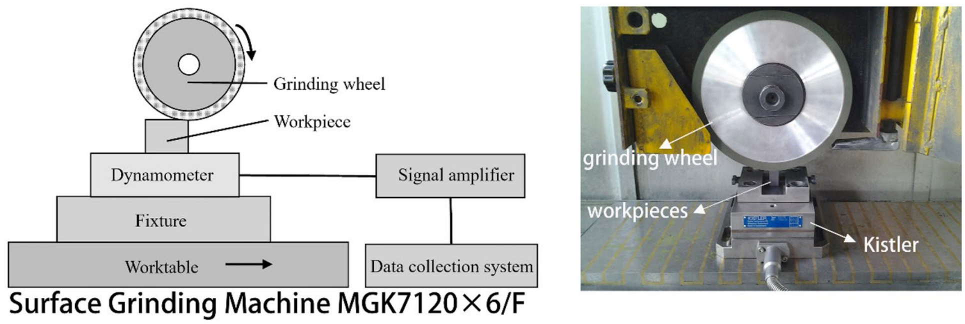

Fig. 3 Silicon nitride ceramic grinding experiment system

workpiece was measured using the MarSurf M300, a portable surface structure measuring instrument.

Due to the continuous impact of abrasive grains, the grinding force signal fluctuated greatly, and there were various interference signals. Therefore, the original signal collected by the dynamometer required high-frequency filtering, and the average value of the signal during the smoothing stage was calculated as the value of grinding force.

3.3 Experiment scheme

The Si_3N_4 grinding experiment adopts the single-stroke plunge-in surface grinding without transverse feed and no spark-out stage. The main grinding parameters that affect the grinding results are selected as follows: the grinding wheel speed v_s, workpiece speed v_w, and grinding depth a_g. As shown in Table 2, the RSM Box-Behnken was used to design the experiment with 3 factors and 3 levels. The experiment scheme is shown in Table 3. For each group of parameters, three repetitive experiments were conducted to minimize the impact of random errors on the experimental results, and the average value of the valid experimental results is eventually taken as the final experiment result used for analysis.

3.4 Result

The surface morphology of the ground Si_3N_4 is as shown in Fig. 4. It can be seen that there are numerous visible grinding grooves on the surface ground by the diamond grinding wheel. For the 1th, 5th, and 7th experiments, there are a large number of brittle removal pits on the surface, which have poor surface quality. For the 4th, 6th, and 8th experiments, the surface is smooth, the abrasive scratch is obvious, and there is no obvious brittle fracture; besides, the plastic upheaval exists.

Table 2 Grinding parameters

Level	v_s/(m·s^{-1})	v_w/(mm·s^{-1})	a_g/μm
−1	10	20	5
0	20	30	10
+1	30	40	15

As shown in Fig. 5a, the ductile regime appears yellow, and the brittle regime appears dark. Since the grinding surface morphologies of the ductile and brittle regimes were completely different in color, the pixel mesh method was used to calculate the proportion of the brittle regime in the observed surface. First, a larger range of 500 μm × 500 μm of the surface morphology image was captured by the digital microscope; then the image was pixel-meshed to automatically calculate the dark color meshes, used as the pixel mesh number of the brittle regimes N_b, as shown in Fig. 5b. The proportion of the brittle regime η can be expressed as

$$\eta = \frac{N_b}{W_c W_p} \times 100\% \tag{8}$$

where W_c and W_p are the numbers of the transverse and longitudinal pixel meshes.

The grinding force F_g is expressed as the combination of the normal force F_n and tangential force F_t. The experiment results of the grinding force F_g, surface roughness Ra, and proportion of the brittle regime η, as well as the material removal mode, are shown in Table 3.

4 Results analysis

4.1 Grinding force and proportion of brittle regime

According to the principle of indentation fracture mechanics, when the abrasive grain is pressed into the ceramic surface at a low speed under the load P, the workpiece undergoes inelastic flow under compressive stress. With the increase of load P, the median crack is initiated just beneath the plastic zone. When unloading, the lateral cracks are caused by the local deformation of the material indentation and pressure field of the median crack. When the lateral crack propagation condition is satisfied, the lateral cracks extend to form the local peeling blocks [7]. The critical load P_c, which leads to the crack propagation, is as shown in Eq. (9) [7].

Table 3 Grinding experiment scheme and results

No	Grinding wheel speed v_s/(m·s^{-1})	Workpiece speed v_w/ (mm·s^{-1})	Grinding depth a_g/μm	Grinding force F_g/N	Proportion of brittle regime (%)	Surface roughness *Ra*/μm	Material removal mode
1	10	20	10	8.959	42.4	1.223	Brittle
2	30	20	10	4.835	5.3	1.056	Ductile
3	10	40	10	11.023	65.2	1.626	Brittle
4	30	40	10	6.416	7.4	1.186	Ductile
5	10	30	5	9.237	47.6	1.034	Brittle
6	30	30	5	3.571	3.8	0.765	Ductile
7	10	30	15	13.581	70.1	1.308	Brittle
8	30	30	15	7.648	9.6	0.980	Ductile
9	20	20	5	2.953	3.3	0.710	Ductile
10	20	40	5	5.910	6.3	0.857	Ductile
11	20	20	15	10.462	61.5	1.115	Brittle
12	20	40	15	11.726	67.1	1.207	Brittle
13	20	30	10	8.395	12.4	1.006	Brittle

$$P_c = \lambda_0 \cdot K_{IC} \cdot (K_{IC}/H)^3 \tag{9}$$

where λ_0 is the coefficient, and the value is 20,000 for Si_3N_4 [7].

The value of P_c for Si_3N_4 is 8.12 N. The grinding force F_g is compared with P_c to determine the material removal mode. When F_g is lower than P_c, the lateral crack will not be initiated, and the material removal mode is the ductile regime; otherwise, it is the brittle regime. As shown in Table 3, the values of F_g in the 2nd, 4th, 6th, 8th, 9th, and 10th experiments were smaller than P_c. Therefore, the material removal mode in the above experiments can be considered the ductile removal mode. In other experiments, it is considered the brittle removal mode.

According to the proportion of the brittle regime η, it is called the ductile regime grinding when η is less than 10%; otherwise, it is referred to as the brittle regime grinding [5]. As shown in Table 3, the result is consistent with the results of the grinding force judgment, indicating the correctness of the material removal mode judgment.

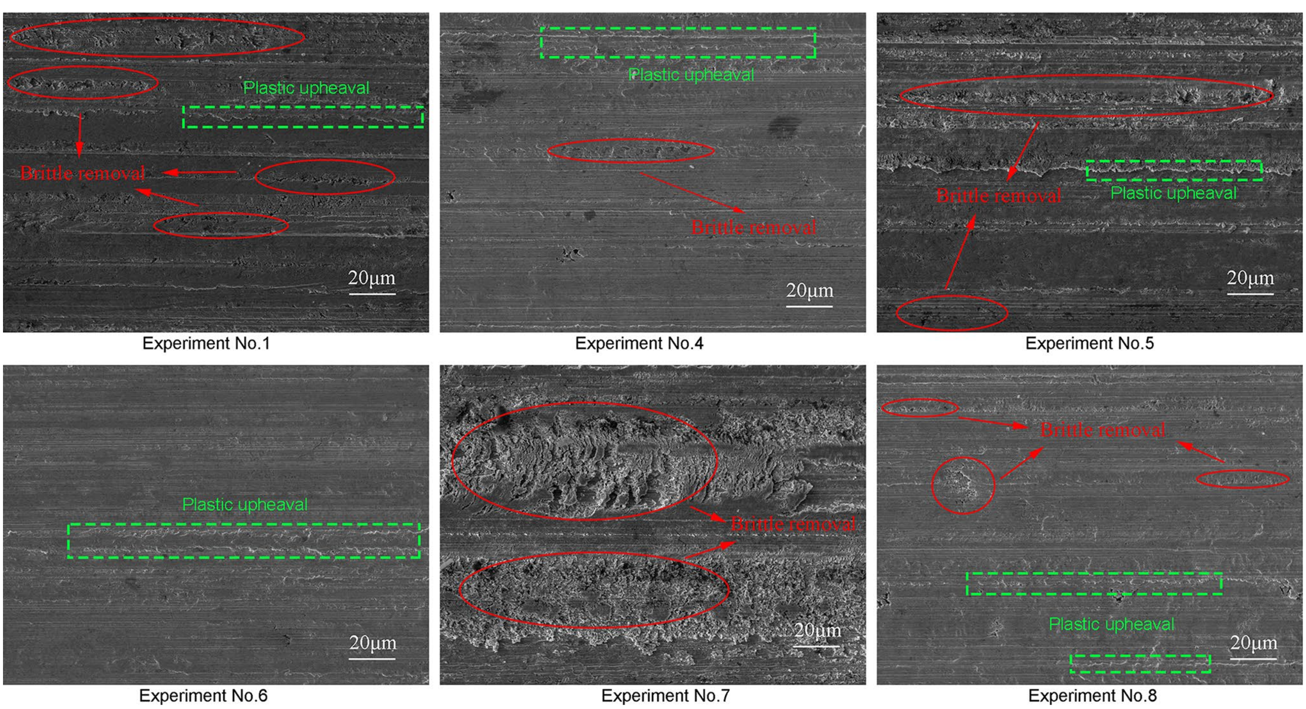

Fig. 4 Surface morphology

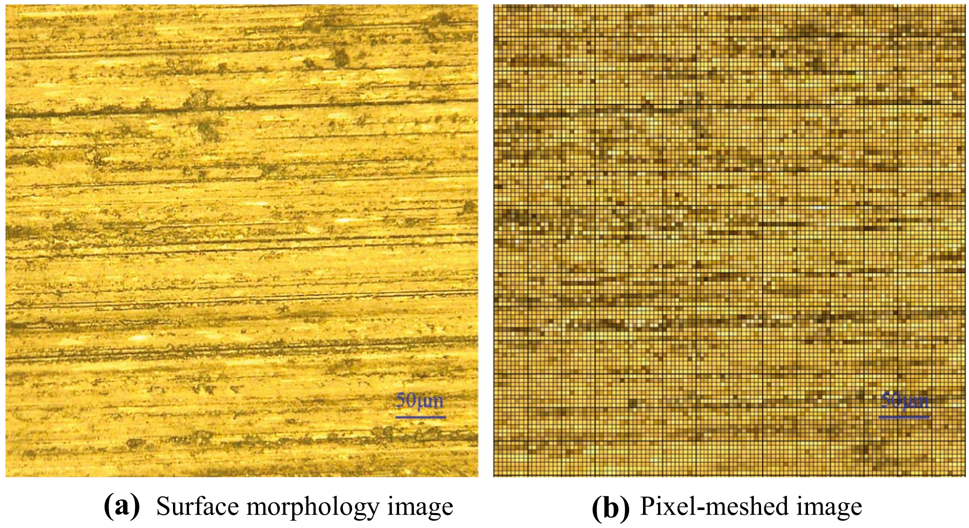

Fig. 5 Pixel mesh of surface morphology: **a** surface morphology image and **b** pixel-meshed image

4.2 Surface roughness

The relationship between F_g and *Ra* was explored, as shown in Fig. 6. It can be seen that the grinding force has great influence on the surface roughness. *Ra* mainly increases with F_g. As F_g increases, the proportion of the brittle regime on the workpiece surface increases, producing a rough surface.

The relationship between *Ra* and η was explored, as shown in Fig. 7. *Ra* increases with η. When η is greater than 40%, *R*a is between 1.0 and 1.63; when η is less than 15%, *R*a decreases. Therefore, reducing η can effectively reduce *R*a and improve the grinding surface quality of the workpiece. In other words, to obtain lower surface roughness, the grinding parameters need to be properly adjusted to achieve the ductile regime grinding, which is consistent with the results of Li et al. [22] and Xiao et al. [23].

As shown in Fig. 4, the brittle removal generates a large number of fracture pits and cracks on the workpiece surface, which makes the surface roughness larger. However, the fracture pits are significantly reduced in the ductile removal surface, so the surface roughness is lower.

4.3 Effect of grinding strain rate

In the experiment, the grain size of the grinding wheel was 150 μm, and the average distance among grains was 175 μm. Then the inter-grain spacing λ was chosen to be twice the average distance, which was 350 μm. The coefficient *K* was 0.72. The maximum undeformed abrasive thickness, grinding strain rate and critical grinding depth prediction were calculated according to Eqs. (1), (6), and (7), as shown in Table 4.

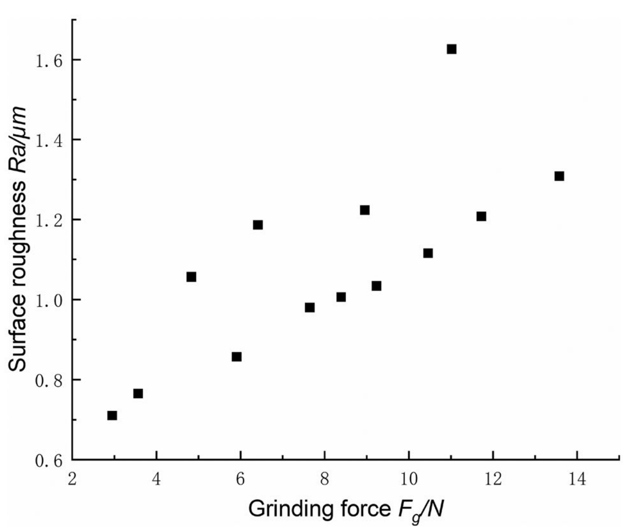

Fig. 6 Relationship between F_g and *Ra*

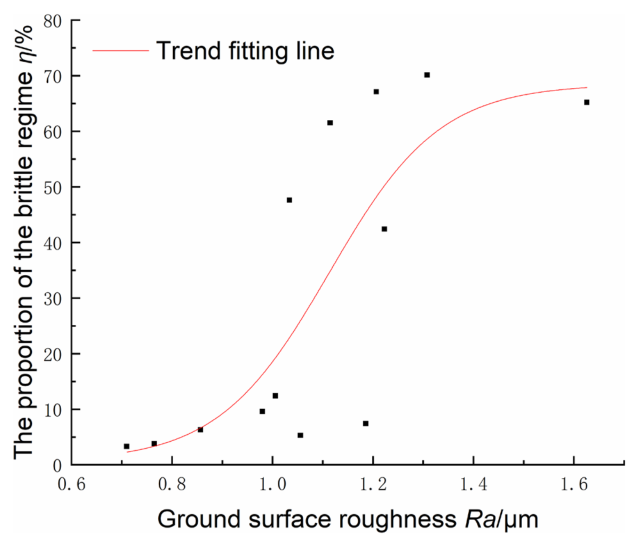

Fig. 7 Relationship between *Ra* and η

Table 4 Prediction results

No.	Strain rate ($\times 10^5$ s^{-1})	Maximum undeformed abrasive thickness a_{gmax} (μm)	Critical grinding depth prediction a_{gd} (μm)	Material removal mode
1	0.79	0.1414	0.0047	Brittle
2	7.08	0.0471	0.2349	Ductile
3	0.39	0.2828	0.0038	Brittle
4	3.54	0.0942	0.1251	Ductile
5	0.74	0.1500	0.0033	Brittle
6	6.7	0.0500	0.2242	Ductile
7	0.43	0.2598	0.0021	Brittle
8	3.83	0.0870	0.1366	Ductile
9	4.44	0.0500	0.1575	Ductile
10	2.22	0.1000	0.7062	Ductile
11	2.57	0.0866	0.0858	Brittle
12	1.28	0.1732	0.0261	Brittle
13	2.09	0.1061	0.0648	Brittle

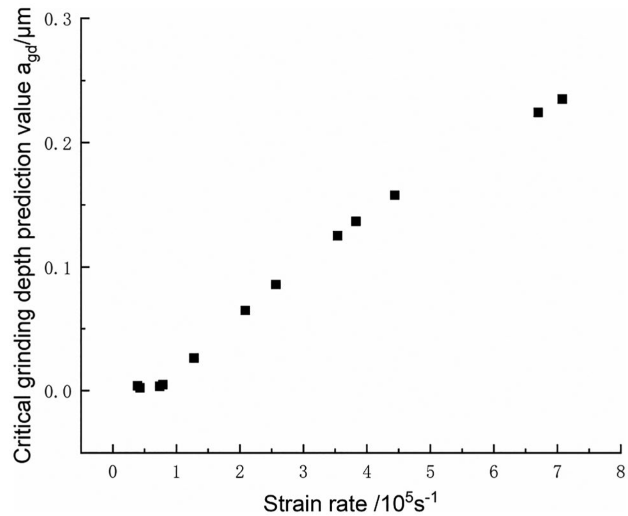

Fig. 9 Variation of critical grinding depth with strain rate

The relationship between the grinding strain rate and η is shown in Fig. 8. η decreases rapidly with the increase of $\dot{\varepsilon}$. But when $\dot{\varepsilon}$ increases consistently, η reaches a stable value, and the material removal mode is mainly ductile removal. At the same time, a_{gd} increases with $\dot{\varepsilon}$, as shown in Fig. 9. This phenomenon is due to the increase of the strain rate in the grinding zone, which increases the deformation speed of the workpiece material, reduces the interaction time between the abrasive grain and workpiece, and weakens the mutual compression. Finally, the toughening mechanism of the material is generated, and the resistance of the crack formation is enhanced.

4.4 Prediction and experimental verification

According to the relationship between a_{gmax} and a_{gd}, the material removal mode can be predicted. When $a_{gmax} \leq a_{gd}$, the grinding process is considered the ductile regime grinding; otherwise, it is the brittle regime grinding. The result is shown in Table 4.

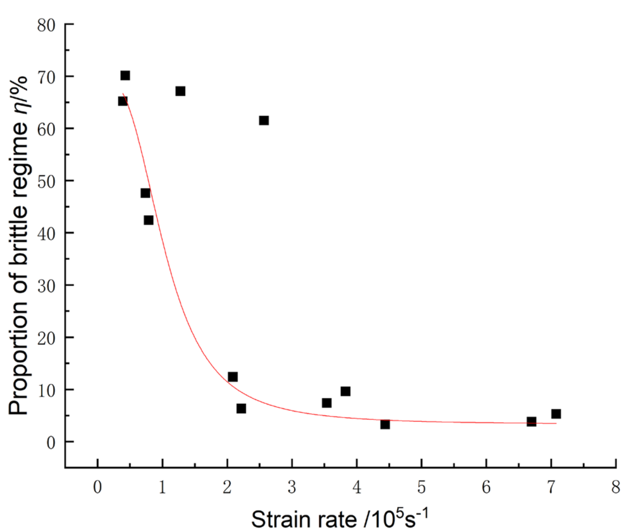

Fig. 8 Trend of brittle regime removal ratio with strain rate

Comparing the removal modes of Si_3N_4 in Tables 3 and 4, they are consistent. In the 2nd, 4th, 6th, 8th, 9th, and 10th experiments, the material removal mode is the ductile removal, and in the remaining experiments, it is brittle removal. Thus, the correctness of the dynamic critical grinding depth model is verified, and the material removal mode of Si_3N_4 under certain grinding parameters can be accurately predicted.

5 Conclusions

This paper has established the dynamic critical grinding depth model of the ductile regime grinding, which is related to the grinding parameters and workpiece material properties. The major conclusions are as follows:

1. based on the classical critical grinding depth model, a dynamic critical grinding depth model is established to guide the actual grinding process;
2. the material removal mode of Si_3N_4 was analyzed by comparing the grinding force F_g with P_c. Furthermore, the material removal mode was determined by the proportion of the brittle regime η;
3. for the Si_3N_4 grinding, the increase of the grinding strain rate can improve the fracture toughness of Si_3N_4 and increase a_{gd}, then the ductile removal is conducive to achieve, and thus the grinding quality of the workpiece can be improved;
4. the maximum undeformed grinding thickness and dynamic critical grinding depth model were used to predict the material removal mode, and the results were consistent with the experiment results.

Author contribution Wei Liu and Zhaohui Deng developed the idea for the study, Rentong Liu, Dubo Tang, Hao Gu, and Shun Liu did the analyses, and Dubo Tang and Wei Liu wrote the paper.

Funding The authors would like to thank the National Natural Science Foundation of China (grant no. 51505144), the Natural Science Foundation of Hunan Province (grant no. 2020JJ5178 and 2020JJ4024), the Scientific Research Fund of Hunan Provincial Education Department (grants no. 20A202), the Open Foundation of Hunan Key Laboratory of Design and Manufacture of Electromagnetic Equipment (grant no. DC201901), and the Open Foundation of Hunan Provincial Key Laboratory of High Efficiency and Precision Machining of Difficult-to-Cut Material (grant no. E21849) for the financial support.

Availability of data and materials The authors confirm that the data and materials supporting the findings of this study are available within the article.

Declarations

Ethics approval This article has not been published or submitted elsewhere.

Competing interests The authors declare no competing interests.

References

1. Liu W, Deng ZH, Shang YY, Wan LL (2019) Parametric evaluation and three-dimensional modelling for surface topography of grinding wheel. Int J Mech Sci 155:334–342. https://doi.org/10.1016/j.ijmecsci.2019.03.006
2. Wu CJ, Li BZ, Liang SY (2016) A critical energy model for brittle–ductile transition in grinding considering wheel speed and chip thickness effects. Proc Inst Mech Eng B J Eng Manuf 230(8):1372–1380. https://doi.org/10.1177/0954405416654194
3. Bifano TG, Dow TA, Scattergood RO (1991) Ductile-regime grinding: a new technology for machining brittle materials. J Eng Ind Trans ASME 113(2):184–189. https://doi.org/10.1115/1.2899676
4. Wang W, Wang ZX, Yao P, Zhang YL, Liu XT (2021) Ductile-brittle transition mechanisms of amorphous glass subjected to taper grinding experiment. Ceram Int 47(2):1844–1854. https://doi.org/10.1016/j.ceramint.2020.09.013
5. Blake PN, Scattergood RO (1990) Ductile-regime machining of germanium and silicon. J Am Ceram Soc 73(4):949–957. https://doi.org/10.1111/j.1151-2916.1990.tb05142.x
6. Venkatachalam S, Li X, Liang SY (2009) Predictive modeling of transition undeformed chip thickness in ductile-regime micro-machining of single crystal brittle materials. J Mater Process Technol 209(7):3306–3319. https://doi.org/10.1016/j.jmatprotec.2008.07.036
7. Chen MJ, Zhao QL, Dong S, Li D (2005) The critical conditions of brittle-ductile transition and the factors influencing the surface quality of brittle materials in ultra-precision grinding. J Mater Process Technol 168(1):75–82. https://doi.org/10.1016/j.jmatprotec.2004.11.002
8. Cheng J, Gong YD, Yan XQ, Zheng WS (2013) Modeling and experimental study of complex critical condition for ductile-regime micro-grinding of hard brittle material. J Mech Eng 49(23):191–198. https://doi.org/10.3901/JME.2013.23.191
9. Ma LJ, Gong YD, Gu LC, Wang H, Tian JC, Li L (2017) Mechanism of surface forming in grinding machinable glass ceramics. J Mech Eng 53(15):201–207. https://doi.org/10.3901/JME.2017.15.201
10. Pratap A, Patra K, Dyakonov AA (2019) Experimental analysis of ductile-brittle transitions for parallel and intersecting micro-slot grinding in BK-7 glass. Ceram Int 45(8):11013–11026. https://doi.org/10.1016/j.ceramint.2019.02.185
11. Singh A, Solanki D, Sencha R, Singh RK, Mote RG, Singh RK (2020) Study and characterization of the ductile-brittle transition zone in sintered zirconia. J Manuf Process 58:749–762. https://doi.org/10.1016/j.jmapro.2020.08.057
12. Zheng ZD, Huang K, Lin CT, Zhang JG, Wang K, Sun P, Xu JF (2022) An analytical force and energy model for ductile-brittle transition in ultra-precision grinding of brittle materials. Int J Mech Sci 220:107107. https://doi.org/10.1016/j.ijmecsci.2022.107107
13. Zhao PY, Zhou M, Zhang YJ, Qiao GC (2018) Surface roughness prediction model in ultrasonic vibration assisted grinding of BK7 optical glass. J Cent South Univ 25(2):277–286. https://doi.org/10.1007/s11771-018-3736-5
14. Liu W, Deng ZH, Shang YY, Wan LL (2017) Effects of grinding parameters on surface quality in silicon nitride grinding. Ceram Int 43(1):1571–1577. https://doi.org/10.1016/j.ceramint.2016.10.135
15. Malkin S, Guo C (2008) Grinding technology: theory and application of machining with abrasives. Industrial Press Inc., New York
16. Neo WK, Kumar AS, Rahman M (2012) A review on the current research trends in ductile regime machining. Int J Mech Sci 63(5):465–480. https://doi.org/10.1007/s00170-012-3949-y
17. Li P, Chen SY, Xiao H, Chen ZQ, Qu M, Dai HF, Jin T (2020) Effects of local strain rate and temperature on the workpiece subsurface damage in grinding of optical glass. Int J Mech Sci 182:105737. https://doi.org/10.1016/j.ijmecsci.2020.105737
18. Huang P, Zhang JQ (2020) Strain rate effect on the ductile brittle transition in grinding hot pressed SiC ceramics. Micromachines (Basel) 11(6):545. https://doi.org/10.3390/mi11060545
19. Wan LL, Deng ZH, Deng ZH (2019) Research and prospect of SHPB experiments for brittle materials. J Mater Sci Eng 37(2):316–324. https://doi.org/10.14136/j.cnki.issn1673-2812.2019.02.028
20. Ding Z, Li B, Liang SY (2015) Maraging steel phase transformation in high strain rate grinding. Int J Adv Manuf Technol 80(1):711–718. https://doi.org/10.1007/s00170-015-7014-5
21. Ravichandran G, Subhash G (1995) A micromechanical model for high strain rate behavior of ceramics. Int J Solids Struct 32(17–18):2627–2646. https://doi.org/10.1016/0020-7683(94)00286-6
22. Li P, Jin T, Xiao H, Chen ZQ, Qu M, Dai HF, Chen SY (2020) Effects of wheel speed on surface/subsurface damage characteristics in grinding of glass-ceramics. Ceram Int 46(11):17717–17728. https://doi.org/10.1016/j.ceramint.2020.04.076
23. Xiao HP, Chen Z, Wang HR, Wang JH, Zhu N (2018) Effect of grinding parameters on surface roughness and subsurface damage and their evaluation in fused silica. Opt Express 26(4):4638–4655. https://doi.org/10.1364/OE.26.004638